International Journal of Mechanical Engineering and Applications
2021; 9(6): 113-131
http://www.sciencepublishinggroup.com/j/ijmea
doi: 10.11648/j.ijmea.20210906.14
ISSN: 2330-023X (Print); ISSN: 2330-0248 (Online)

Dynamical Investigation of Cam-Follower Profile Under Space - 100 to + 120°C Temperature Condition

Jafar Keighobadi[1], Hojjat Fouladi[1], Davood Hashempour[2], Amirreza Rafat Talebi[1]

[1]Department of Mechanical Engineering, University of Tabriz, Tabriz, Iran

[2]Space Exploration Research Center, Iranian Space Research Center, Tabriz, Iran

Email address:

Keighobadi@tabrizu.ac.ir (J. Keighobadi), Folady1994@gmail.com (H. Fouladi), d.hashempour@isrc.ac.ir (D. Hashempour), Amirreza.t.r@gmail.com (A. R. Talebi)

To cite this article:

Jafar Keighobadi, Hojjat Fouladi, Davood Hashempour, Amirreza Rafat Talebi. Dynamical Investigation of Cam-Follower Profile Under Space - 100 to + 120°C Temperature Condition. *International Journal of Mechanical Engineering and Applications*. Vol. 9, No. 6, 2021, pp. 113-131. doi: 10.11648/j.ijmea.20210906.14

Received: November 7, 2021; **Accepted**: December 14, 2021; **Published**: December 24, 2021

Abstract: Cam-follower mechanism efficiency in production of desired motions has been proved along the history of space missions. In this paper, according to pre-specified spatial condition of wide temperature variations between -100 and +120 Celsius degrees, some new and innovative cam-follower profile designs are presented. In the first follower mechanism, through rotating a connected screw to a servomotor, changes in length of the moving follower on cam is compensated with respect to the temperature changes of certain spatial conditions. In the second design, an inclined surface cam is equipped with an active controllable follower. As the third suggestion, the design with an inclined cam surface is optimized by investigating the length of the shaft connected to the cam. In the fourth model, a new design is proposed by changing the shaft's material from aluminum to titanium and a modified design is presented. The proposed designs are investigated and compared using the analytical solutions and optimization tools using MATLAB and ANSYS. The purpose of this study was to identify the effect of profile type on the dynamic behavior of the mechanism under the effects of a temperature difference of -100 to +120°C in space condition. It is concluded that changing the length of the follower, using an inclined cam surface and optimizing the length of the shaft connected to the follower are all effective solutions to the cam's volume variation problem. The results also indicate that for solving the problem of the volume variation of the cam-follower mechanism a combination of the proposed designs is optimal. Moreover, among the presented designs, the mechanism with an inclined cam surface with an aluminum shaft is shown to have the highest precision and performance with respect to the other three.

Keywords: Cam-Follower Mechanism, Temperature Changes, Spatial Conditions, Profile Modification, Mechanism Design

1. Introduction

Cam-follower mechanism with numerous industrial applications includes different type and shape according to its variant areas in industry. The utilization of this mechanism is carried out regarding wide-spread purposes and trends. For instance, attaining precise motion, reducing the intensity of contact stresses forces and regulation or reduction of vibrations in joints and elements. There are multiple factors that should be analyzed in this subject, such as the material dedicated for the cam design, type of the follower/cam, the shape of cam profile, and the eccentricity intensity as well. A very essential aspect of the cam- follower mechanism design is known the cam profile with major effects on the aforementioned purposes. Cams as a group of machine elements produce required motions as a result of continuous contacting by the follower component. The frequent exploiting and the essentiality of cam-followers in machines is a result of the possibility of changing the motion quality of the follower easily with the change of cam shape. Moreover, in a single motion cycle of a cam the follower can be given a variety of motions e.g., constant velocity motion, constant acceleration etc. Cam-follower mechanism is a widely used mechanical system in the design of mechanical systems. This mechanism can be found in automobile engines, automatic looms and the industrial food machinery. This mechanism is used for the conversion of the rotary motion into the reciprocal and oscillatory motions. In addition, this

mechanism is widely used in the aerospace industry and the space stations and satellites for the opening and closing of the antennas and solar panels. Temperatures in space can range from the extremely cold, hundreds of degrees below freezing, to hundreds of degrees above – especially if a spacecraft ventures close to the Sun. Although there is no air in space, energy is carried by radiation, usually coming from the Sun, that causes heating when it is absorbed by spacecraft, planets or other celestial bodies. The mechanism that are inside the spacecraft are affected by these drastic temperature variations as well [1]. These temperature variations will result in mechanical and technical difficulties in the mechanism functionalities. Hence, solving these malfunctions are indispensable in the space industry and have made these industries to spend billions of dollars to optimize the designs that can handle and endure the thermal variations. As mentioned before, Cam-follower mechanism is among the widely used mechanisms in the space industry and therefore, the studies conducted on the cam volume variations are vital since the volume variation causes variations on the displacement, velocity and the acceleration and obtaining these variations will assist in the design of much more improved and subtle mechanism. Hence, by acquiring the displacement, velocity and the acceleration a better understanding of the cam-follower mechanism in space conditions can be accomplished. This helps in the reduction of the space satellite's imprecision in different missions such as the satellite imagery of the earth's surface. In the latter, even a seemingly negligible imprecision such as 0.1 percent during the antenna opening can end up in a multi-kilometer inaccuracy in the satellite imagery of the desired location. Hrones is among the first researchers to investigate the cam dynamics [1]. This research is a theoretical approach and the results were compared with the Mitchell's experimental data [2]. Followed by Hrones and Mitchell's research, the researchers have approached the simultaneous kinematic and dynamic analysis of the cam mechanism like Dudley [3] and Stoddart [4]. Later, Kwakernaak and Smit presented a technic for the optimal design of the mechanism [5]. Hong-Sena and Wen-Teng did analysis on the curvature of spatial cam-follower mechanisms [6]. in the mentioned paper the contact of the surfaces of cam and follower are considered linear. Next, Lindholm and Björklund mentioned and characterized wear on cam-follower systems [7]. The mentioned paper depicted the application of one of the most crucial contact surface of a modern composite system. Three years later, Kyung and Sacks analyzed the behavior of cam-follower mechanisms and the Geneva mechanism and their displacement diagrams [8]. Kyung and Sacks presented a center parametric algorithm for mechanical structures. Koser studied a cam mechanism for gravity-balancing [9]. The conducted study is related to the gravitational compensation of a certain type of cam. Jianpinga and Zhaoping did a parametric design and motion analysis for a line translating tip follower cam mechanism based on the model datum graph [10]. In their paper it is found that the cam mechanism can present the anticipated motion laws using the follower in contact with the higher pair. Hsieh designed and analyzed a Geneva mechanism with curved slots [11]. The Geneva mechanism is the most frequently used among the other mechanisms in the intense space conditions. Willemot and Thoreson modeled shoulder instability as a cam follower mechanism [12]. In their research, a simple glenohumeral joint is used as a stimulated experimental cam-follower mechanism model when in translation. Safaeifar designed a cam-follower mechanism and analysed it [13]. It is mentioned in the previous paper that a cam is a member of a machine that translates motion to another member using its irregular shape. Hejima and Svoboda analyzed a cam-follower mechanism with a presented methodology for choosing a suitable electric motor and a proper selection of coil springs [14]. They stated many applications of the cam-follower mechanism such as Combustion engines. Lin and Hou presented a cam mechanism for minimizing the torque fluctuation of engine camshafts [15]. They suggested the design and testing of the suspension mechanism to minimize the oscillations of the torques of the motors of the cam axis. Khonsari and Torabi presented a line contact thermo-elasto-hydro-dynamics analysis of studying the cam-and- follower contact [16]. The work was done for the purpose of analyzing the linear thermo elastohydrodynamic and the behavior of the cam-follower contact. Karamis and Cerit studied the effects of different ceramic size and fraction on wear behavior of A1 matrix composites in automobile cams [17]. A number of metal matrix composites are made for determining their thermography. Also there has been many researches conducted for designing controller for thermal and non-linearity disturbances that can be used as references in designing controllers for the cam-follower mechanism. For example, Keighobadi et al. for design of a nonlinear disturbance rejection–based controller for the robust output regulation of a triaxial microelectromechanical system (MEMS) gyroscope [18], extended state observer surface control [19]. Further new immersion and invariance observer for inertial MEMS attitude-heading reference systems, an enhanced fuzzy H∞ estimation algorithm [20, 21] and nonlinear disturbance rejection–based controller of a triaxial MEMS vibratory gyroscope [22, 23] are presented. The nonlinear control [24-30], linear and nonlinear observer and filters [31-40] and predictive techniques [41-43] properly explained space mechanism related control systems.

As presented, there has been many researches on the optimal design of cam- follower mechanism and the methods have evolved with time. For the general applications, the typical classic methods are efficient for obtaining the desired results. However, in special conditions like the conditions of our problem, rendering state-of-the-art methods are necessary. In this study the dynamic response of the cam-follower mechanism is investigated for different types of cam profiles used in previous research documents. The dynamics of the high velocity cam-follower mechanisms have been an indispensable matter for the researchers. As mentioned, there has been several researches on the cam-follower mechanisms and the effects of temperature on a number of materials.

However, to the best of the authors' knowledge, to this day, there has not been any studies on the effects of temperature on the cam-follower mechanisms performance. Hence, the presented methods in this study are brand new and used in this research for the first time. To identify the effects of the temperature, it is assumed that the dimensions of the mechanism parts are known. So, the main purpose is to produce some standard profiles according to the dimensions and even type of the cam's motion. It should be noted that in this study the cam is supposed to have only one type of motion and as a result, only the standard profiles has been investigated. Using multiple dimension sets, multiple types of motions and their combinations, an infinite number of cam profiles can be designed. In this research, the cam profiles are produced using same dimensions but with different motions will be generated to have a comparative approach between the different profiles.

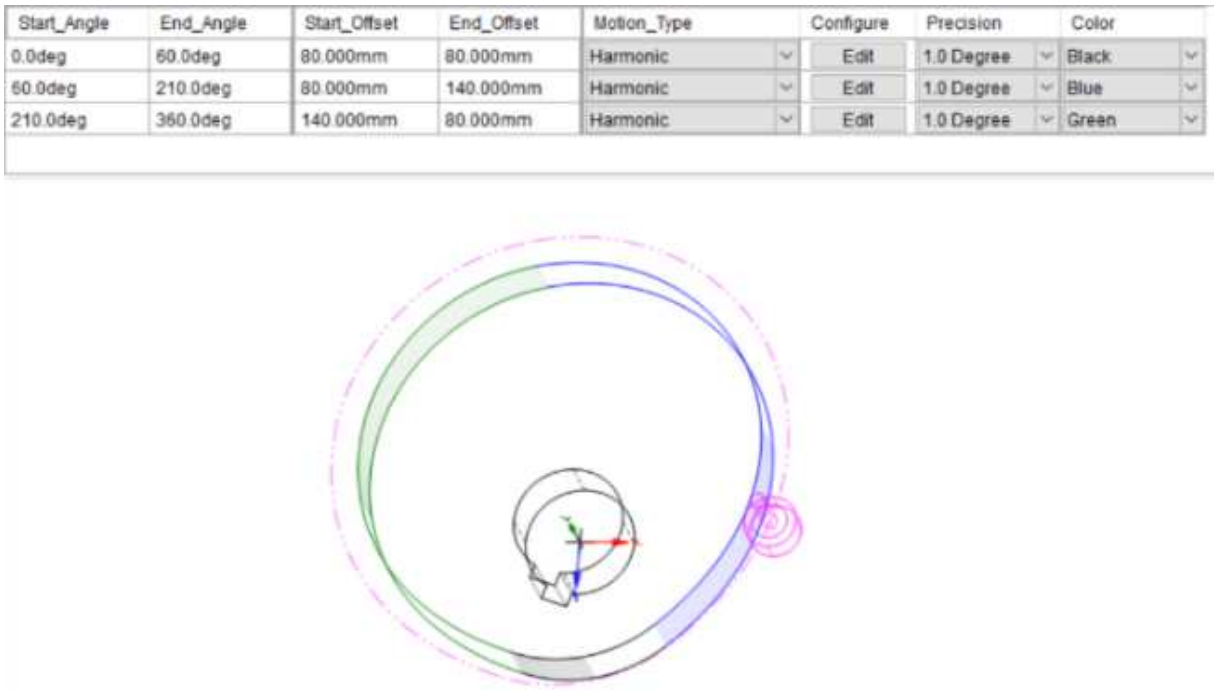

Figure 1. *The assumed initial cam profile.*

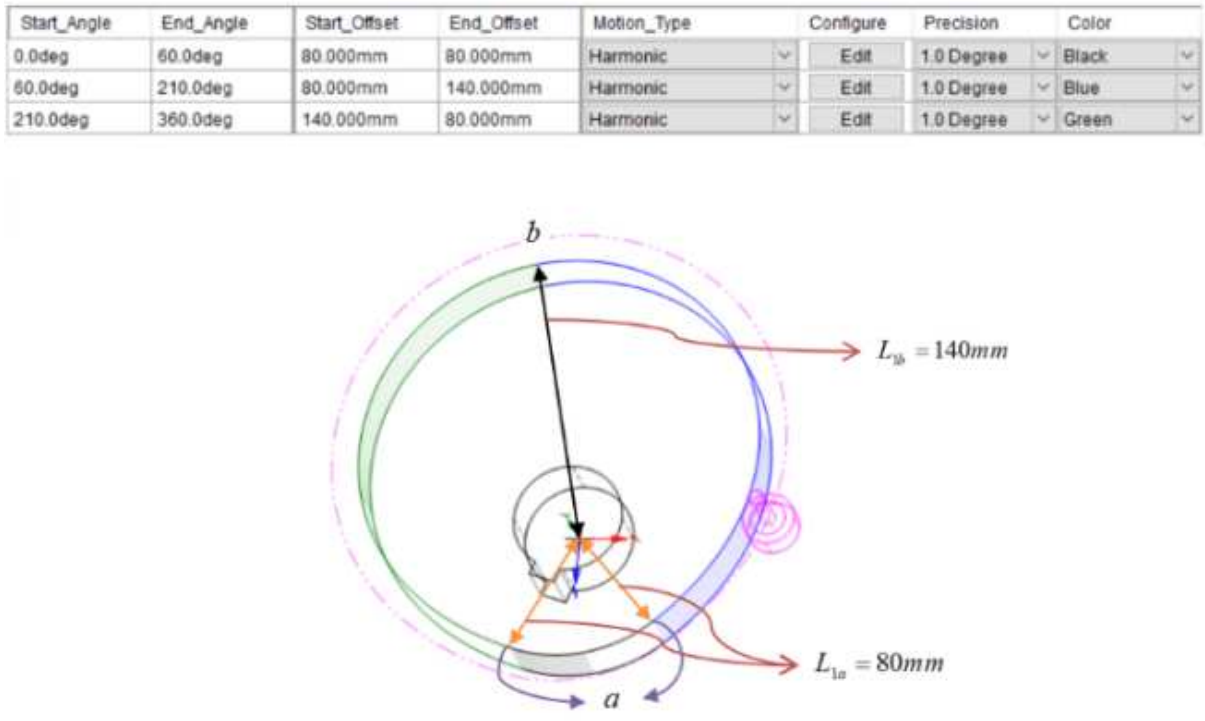

Figure 2. *The positions of the assumed dimensions.*

Start_Angle	End_Angle	Start_Offset	End_Offset	Motion_Type	Configure	Precision	Color
0.0deg	60.0deg	79.768mm	79.768mm	Harmonic	Edit	1.0 Degree	Black
60.0deg	210.0deg	79.768mm	139.594mm	Harmonic	Edit	1.0 Degree	Blue
210.0deg	360.0deg	139.594mm	79.768mm	Harmonic	Edit	1.0 Degree	Green

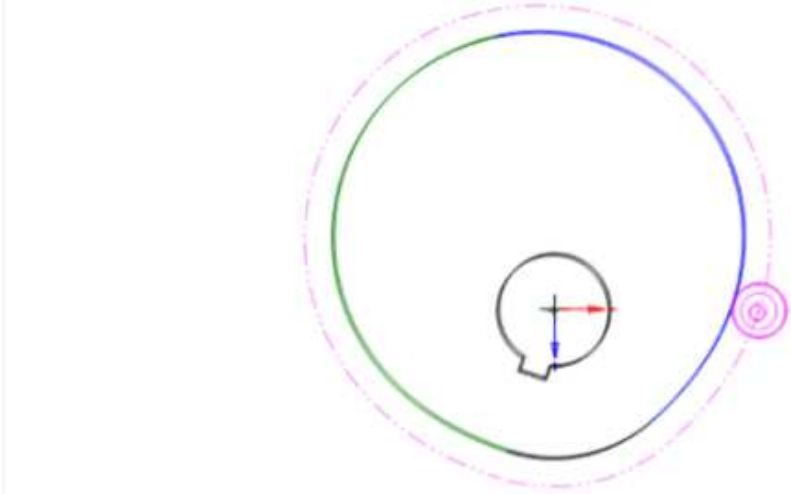

Figure 3. *The cam profile at the lowest temperature.*

Start_Angle	End_Angle	Start_Offset	End_Offset	Motion_Type	Configure	Precision	Color
0.0deg	60.0deg	80.176mm	80.176mm	Harmonic	Edit	1.0 Degree	Black
60.0deg	210.0deg	80.176mm	140.309mm	Harmonic	Edit	1.0 Degree	Blue
210.0deg	360.0deg	140.309mm	80.176mm	Harmonic	Edit	1.0 Degree	Green

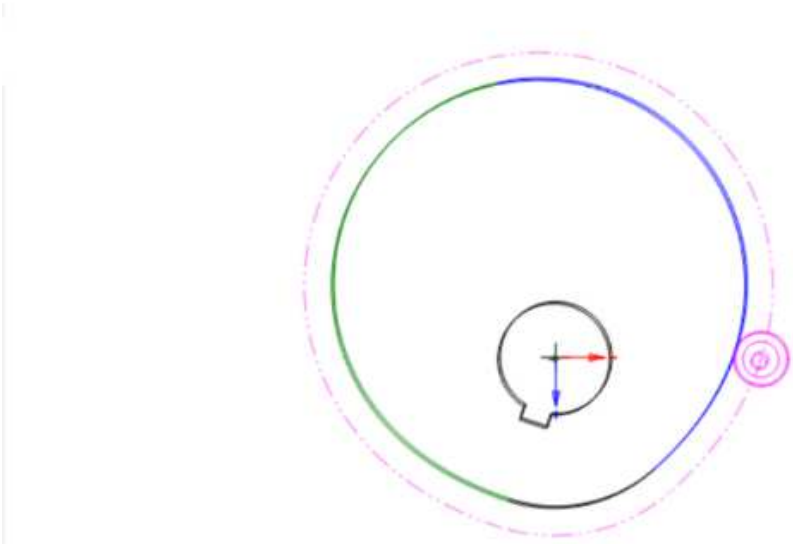

Figure 4. *The cam profile at the highest temperature.*

2. Cam-Follower Model

The assumed initial cam profile using all three materials, namely 7075 Aluminum T6, Titanium and the stainless steel are depicted in Figure 1. As shown in the figure 1 and the table on its top, harmonic motions and arbitrary dimensions at standard temperature 25℃ are considered.

In the following eq. (1) of representation the relation of thermal expansion, the initial dimensions of the cam L_1 and the coefficient of linear thermal expansion α for the considered materials in design of the cam mechanism with respect to the temperature variations ΔT, the dimensional variation ΔL is calculated:

$$\Delta L = \alpha L_1 \Delta T \quad (1)$$

The calculations are done with the initial temperature of $T_1 = +25℃$ and the final temperatures $T_2 = -100℃, T_2 = -50℃$, $T_2 = 0℃$, $T_2 = +25℃$, $T_2 = +50℃$ and $T_2 = +120℃$. For aluminum 7075 T6 the following parameters are obtainable:

For example at $T_2 = -100℃$ we can write:

a) $\alpha = 23.2 \times 10^{-6} \frac{1}{℃}$[15], $T_1 = +25℃$. $L_{1^a} = 80\ mm$:

Hence, according to eq. (1):

$$\Delta L_a = \alpha L_{1^a} \Delta T \quad (2)$$

Where,

$$\Delta L_a = L_{2^a} - L_{1^a} \quad (3)$$

For example, using the given equations and the parameters, $\Delta L_a = -0.232\ mm$

Eq. (3) yields:

$$L_{2^a} = 79.768\ mm$$

Keeping the same final temperature as:

$\alpha = 23.2 \times 10^{-6}\ 1/℃, T_1 = +25℃. L_{1^b} = 140\ mm$:

According to eq. (1), the second materials related changes dimension are obtained as:

$$\Delta L_b = \alpha L_{1^b} \Delta T \quad (4)$$

In other hand:

$$\Delta L_b = L_{2^b} - L_{1^b} \quad (5)$$

Using the given equations and the parameters:

$$\Delta L_b = -0.406\ mm$$

And from the eq. (3) we have:

$$L_{2^b} = 139.594\ mm$$

The cam profile after the temperature increase is illustrated in Figure 2 with details on the points a and b.

It is obvious that change in any point of the cam will result in change of other points position. The cam profile in the temperature $T_2 = -100℃$ is presented in Figure 3. According to the computational results, the cam dimensions are decreased at a rate of 0.29 percent with respect to the initial cam dimensions.

Now assuming $T_2 = +120℃$, a) $\alpha = 23.2 \times 10^{-6} \frac{1}{℃}$[15], $T_1 = +25℃$, $L_{1^a} = 80\ mm$:

similar to the previous section: $\Delta L_a = 0.1763\ mm$

And hence:

$$L_{2^a} = 80.176mm$$

b) $\alpha = 23.2 \times 10^{-6} \frac{1}{℃}$[15], $T_1 = +25℃$, $L_{1^b} = 140\ mm$:

similarly:

$$\Delta L_b = 0.3086\ mm$$

And hence:

$$L_{2^b} = 140.309mm$$

The new cam profile at $T_2 = +120℃$ and its specifications are presented in Figure 4. According to the computational results, the cam dimensions are enlarged at a rate of 0.22 percent with respect to the initial cam dimensions. It is seen that an increase or decrease in the temperature of the work space of the cam mechanism results in the increase or decrease of the cam mechanism total volume.

Since the thermal expansion relation is linear, simplified analysis to eliminate the vagueness caused by the above equations and diagrams is applied. Generally speaking, it can be simply stated that according to the coefficients of linear thermal expansion for the three materials in this study, the titanium's coefficient $\alpha_T = 8.41 \times 10^{-6} \frac{1}{℃}$ is comparatively smaller with respect to the so-called aluminum 7075 T6 with the coefficient $\alpha_A = 23.2 \times 10^{-6} \frac{1}{℃}$, and stainless steel with the coefficient $\alpha_s = 16 \times 10^{-6} \frac{1}{℃}$. Therefore, the dimensional variation of titanium caused by intense temperature variation will be less than the other two. In other words, the volume variation of titanium is significantly small and thus to sum up:

The volume variation caused by temperature variation becomes:

Aluminum 7075 T6 > Stainless steel > Titanium

3. Dimensional Variation of the Mechanism

For the purpose of further investigation of the dimensional varying problem, an example of cam-follower mechanism is assumed in continuous contact with a valve as shown in figures 5, 6 and 7. By temperature rising, the cam mechanism expands which in turn causes the valve movement from its initial position as it is depicted in Figure 6. The opposite of this phenomenon happens when the temperature is decreased. Figure 7 illustrates the case where the temperature is reduced and hence the cam and the valve are out of contact and therefore, an abrupt jump occurs in the valve.

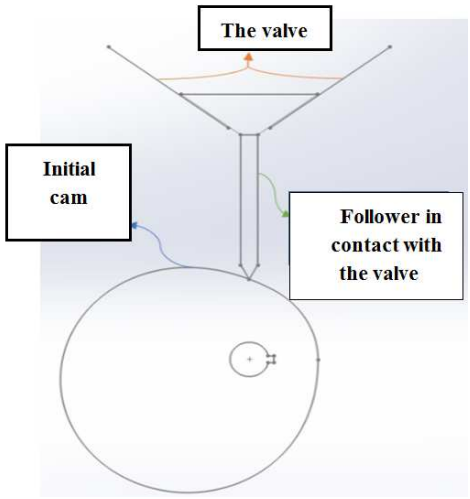

Figure 5. *A cam-follower mechanism in contact with valve.*

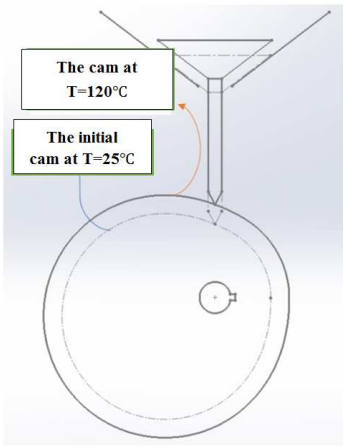

Figure 6. *A cam-follower mechanism in contact with a valve after the temperature rise.*

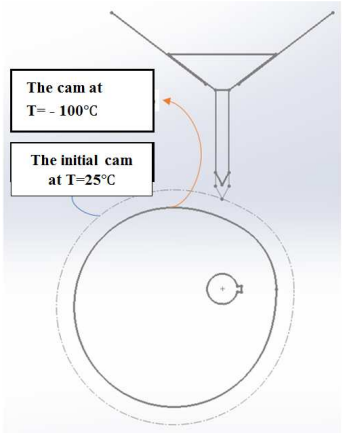

Figure 7. *A cam-follower mechanism in contact with a valve after the temperature drop.*

Start_Angle	End_Angle	Start_Offset	End_Offset	Motion_Type	Configure	Precision	Color
0.0deg	60.0deg	80.000mm	80.000mm	Harmonic	Edit	1.0 Degree	Black
60.0deg	210.0deg	80.000mm	140.000mm	Harmonic	Edit	1.0 Degree	Blue
210.0deg	360.0deg	140.000mm	80.000mm	Harmonic	Edit	1.0 Degree	Green

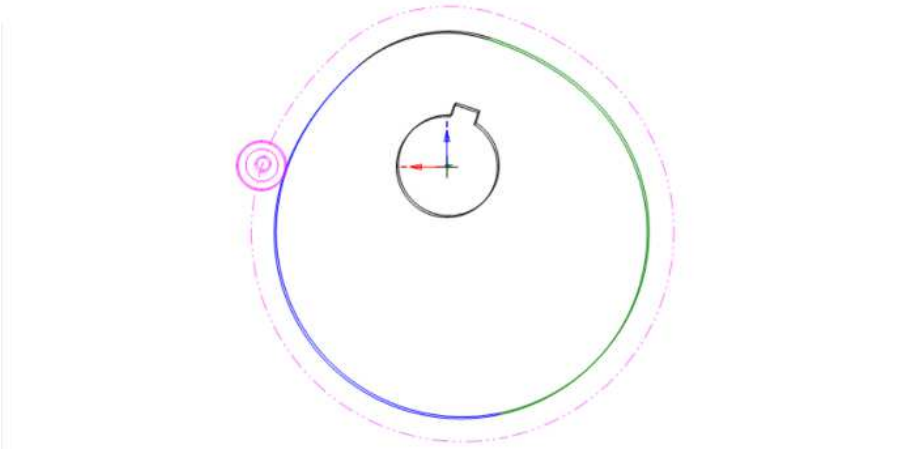

Figure 8. *A cam-follower mechanism with a harmonic motion.*

Start_Angle	End_Angle	Start_Offset	End_Offset	Motion_Type	Configure	Precision	Color
0.0deg	60.0deg	80.000mm	80.000mm	Cycloidal	Edit	1.0 Degree	Black
60.0deg	210.0deg	80.000mm	140.000mm	Cycloidal	Edit	1.0 Degree	Blue
210.0deg	360.0deg	140.000mm	80.000mm	Cycloidal	Edit	1.0 Degree	Green

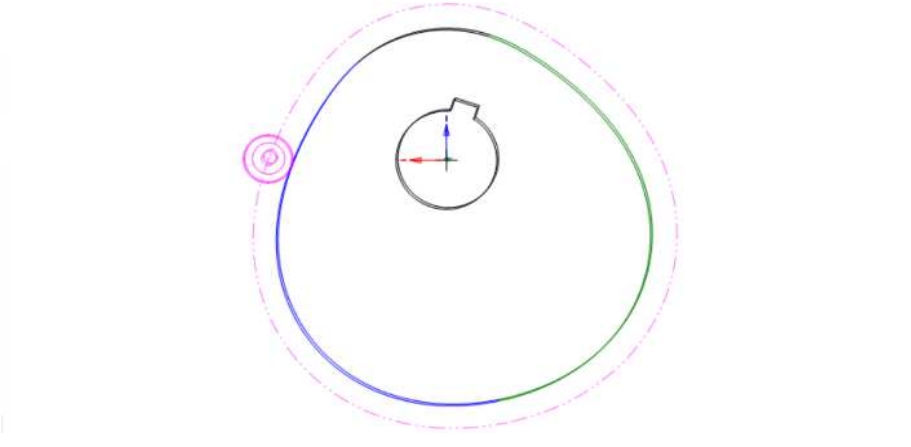

Figure 9. *A cam-follower mechanism with a cycloidal motion.*

Start_Angle	End_Angle	Start_Offset	End_Offset	Motion_Type	Configure	Precision	Color
0.0deg	60.0deg	80.000mm	80.000mm	Constant_Velocity	Edit	1.0 Degree	Black
60.0deg	210.0deg	80.000mm	140.000mm	Constant_Velocity	Edit	1.0 Degree	Blue
210.0deg	360.0deg	140.000mm	80.000mm	Constant_Velocity	Edit	1.0 Degree	Green

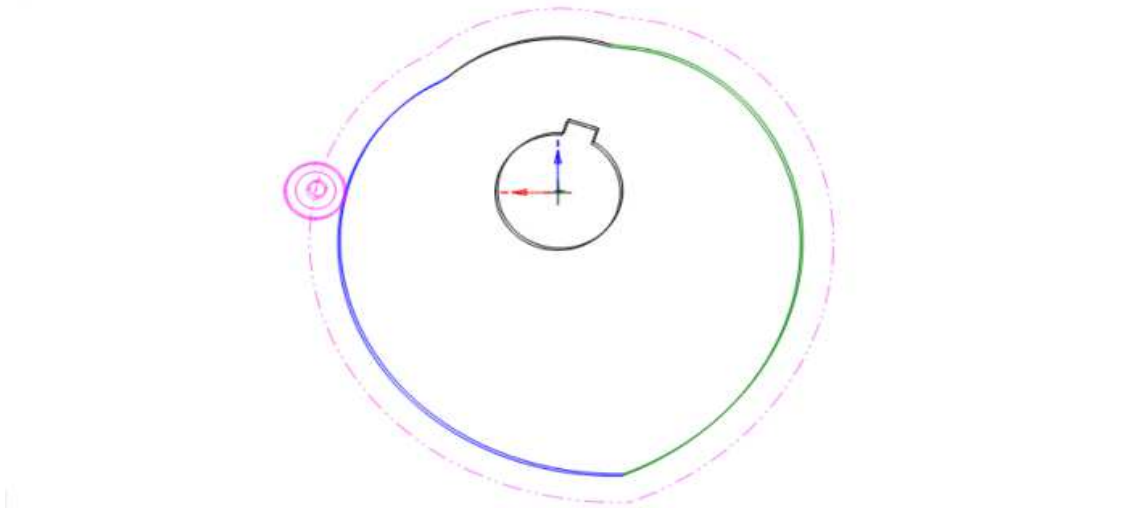

Figure 10. *A cam-follower mechanism with a constant velocity motion.*

4. Overall Motion by Cam-Tax Software

As mentioned in the preceding section, first different motions and their displacement diagrams should be examined to find the prototype in which the dimensional variation caused by temperature changes is the least in comparison to the other materials. To this end, the Cam-tax software is used for this analysis. In Figures 8 to 10, three different cam-follower mechanisms with the same dimensions and different types of motions including, harmonic, cycloidal and constant velocity are depicted through the Cam tax software.

5. Temperature Variation Effect in Cams

Considering adjustable length of the follower in accordance with the environment condition change is the first solution of the difficulty. This means that for the case of temperature rising, the length should be decreased so that the contact won't result in the valves opening. Similarly, in the case of temperature dropping down, the follower's length should be increased to prevent the contact losing between the follower and valve. To apply this solution to the mechanism, a controllable servomotor is attached to the follower as shown in Figure 11. For the control of the servomotor either an open loop or a closed loop framework can be used. For the open-loop case, a system is designed to rotate some certain degree clockwise when the temperature rises and similarly rotation by some certain degree counter-clockwise for compensation of temperature drop. In the closed-loop system case, thermal and position censors are considered to regulating the follower's position with respect to the temperature in the feedback loop through changing the follower's length.

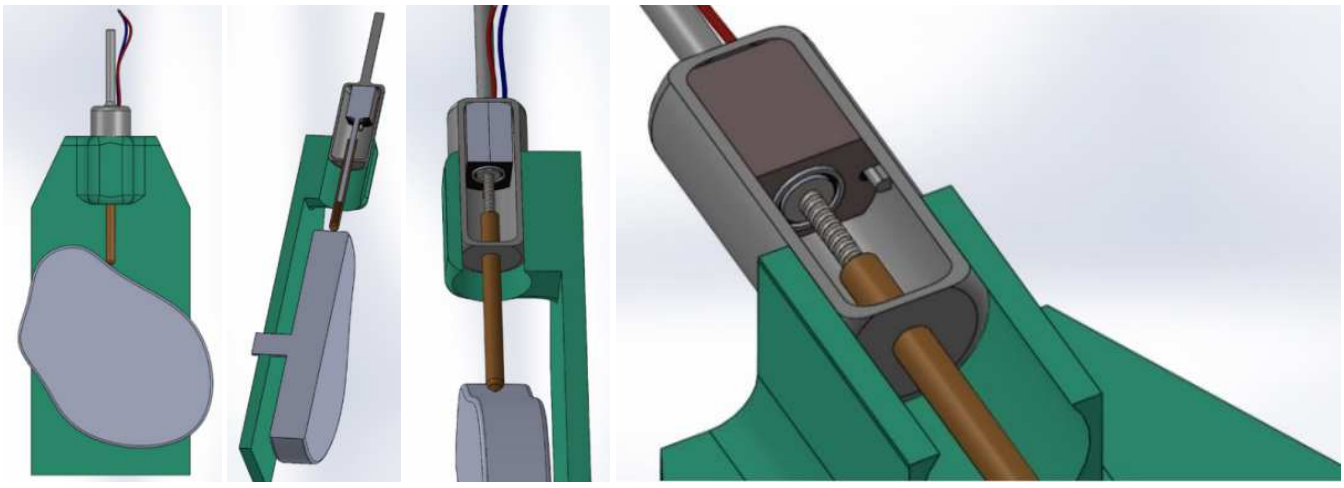

Figure 11. *A cam-follower mechanism with a variable follower length.*

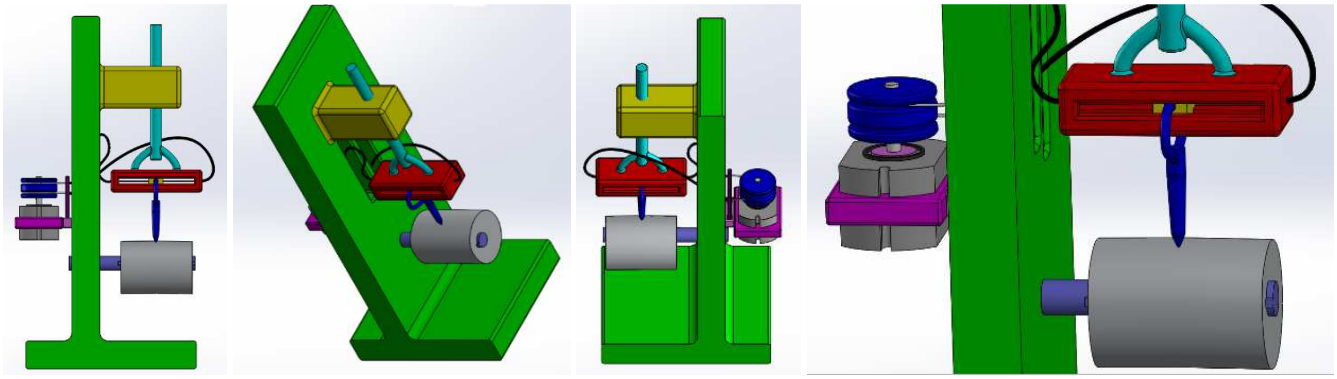

Figure 12. *A depiction of the cam-follower mechanism with a cam with a ramp surface.*

Another solution to the temperature variation problem is the use of a cam with a ramp surface instead of the common surface. The suggested design is depicted in Figure 12. In this design, the follower is initially in contact with the cam's surface at the standard environment temperature. The follower is connected to the servomotor with a number of wires that calculate the follower's position using the position control system in different temperatures. When the temperature rises, the follower slides down the inclined surface of the cam to overcome the change in the cam's dimensions and to make the contact with the cam again. The reverse motion happens by rise of the temperature. When the temperature goes down, the servomotor guides the follower to the top of the cam surface proportionate to the temperature rise to make the follower and cam to be contacted. The reason that this surface with a ramp is barely visible is the negligible difference between the cams top and bottom dimensions that is approximately 0.8 millimeters at its most. Similarly, the two types of closed-loop and open-loop systems can be used for the control of this design.

The best economical design for solving the temperature variation problem is the use of expansion and contraction of metal shafts caused by temperature variations. In this design, an aluminum 7075 T6 shaft, the same as the cam's material is chosen. The reasons behind this choice are the strength and the high coefficient of linear thermal expansion of the material. Figure 13 illustrates the design.

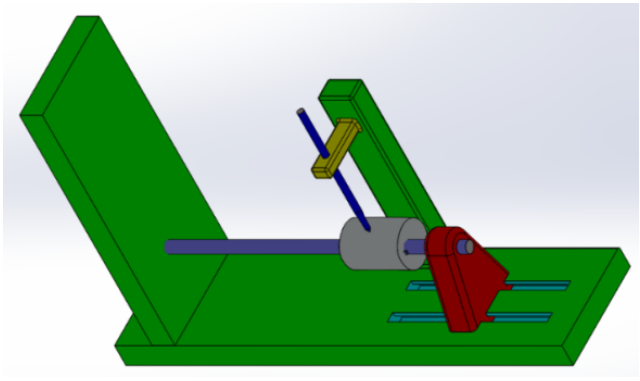

Figure 13. *A design for optimizing the length of a shaft connected to a cam with a ramp surface.*

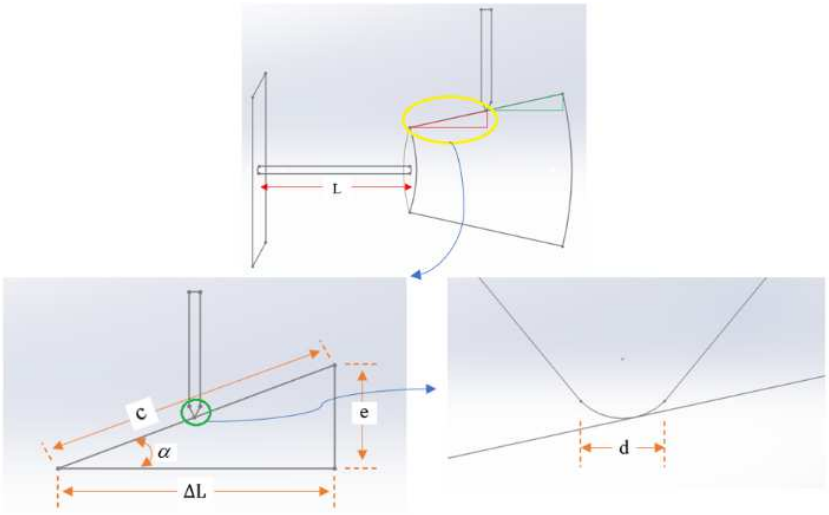

Figure 14. *The defined parameters used in the design of the proposed mechanism.*

As it is presented in the Figure 12, a hinged support is connected to the cam's shaft to prevent the shaft from oscillation while rotating. The parameters shown in Figure 12 are the length L of the shaft connected to the cam and the diameter of tip of the valve, d. Furthermore, e is obtained as follows:

$$e = \alpha_{A_l} L_{1b} \Delta T \quad (6)$$

Since the proposed design is controlled by the shaft, the maximum temperature variation is taken into account in the calculations as:

$$\Delta T = -100 - 25 = -125℃$$

The likelihood of cam and follower in losing of contact due to low temperature requires a precautionary approach. Hence, the temperature difference is assumed to be $\Delta T = -130℃$ for gaining more certainty in the design. The positivity or the negativity of ΔT does not affect the calculations and therefore:

$$e = \alpha_{A_l} L_{1b} \Delta T = 23.2 \times 10^{-6} \times 140 \times 130 = 0.422mm$$

For the shaft:

$$\Delta L = \alpha_{A_l} L \Delta T \quad (7)$$

From the Pythagoras theorem:

$$c^2 = (\Delta L)^2 + e^2 \quad (8)$$

And also:

$$c = d \times f \quad (9)$$

In which f is used as a coefficient to calculate the precision.

Using equations (7) through (9) leads:

$$d^2 \times f^2 = (\alpha_{A_l} L \Delta T)^2 + e^2 \quad (10)$$

Substituting d=0.5 mm:

$$(0.5)^2 \times f^2 = (23.2 \times 10^{-6} \times L \times 130)^2 + (0.422)^2 \quad (11)$$

To find the best values of L and f, the particle swarm optimization (PSO) algorithm of MATLAB method is applied on the following function:

$$fun = (0.5 \times f)^2 - (23.2 \times 10^{-6} \times L \times 130)^2 - (0.44)^2 \quad (12)$$

Given that the coefficient of linear thermal expansion of titanium is less than the coefficient of aluminum 7075 T6, the changes in the dimensions caused by the temperature variations of the titanium cam are less than that of the aluminum. Hence, by choosing aluminum shaft for the titanium cam in the mechanism, a better precision is expected. It should be noted that the subscript T is used to denote the parameters related to the titanium cam. Similar to the previous section:

$$e_T = \alpha_T L_{1b} \Delta T = 8.41 \times 10^{-6} \times 140 \times 130 = 0.153 \text{ mm} \quad (13)$$

$$\Delta L_T = \alpha_{A_l} L_T \Delta T \quad (14)$$

And similarly:

$$c_T{}^2 = (\Delta L_T)^2 + e_T{}^2 \quad (15)$$

In which:

$$c_T = d \times f_T \quad (16)$$

$$d^2 \times f_T{}^2 = (\alpha_{A_l} L_T \Delta T)^2 + e_T{}^2 \quad (17)$$

Using equations (14) through (17):

$$(0.5)^2 \times f_T{}^2 = (23.2 \times 10^{-6} \times L_T \times 130)^2 + (0.153)^2 \quad (18)$$

Using the POS method to obtain the best values for f_T and L_T, the function under optimization becomes:

$$fun = (0.5 \times f_T)^2 - (23.2 \times 10^{-6} \times L_T \times 130)^2 - (0.153)^2 \quad (19)$$

Time in Degrees (Harmonic)	Displacement (mm) at -100 °C	Velocity (m/sec) at -100 °C	Acceleration (m/sec^2) at -100 °C
30	79.7680	0.0000	0.0000
60	79.7680	0.0000	1.7005
90	85.4809	0.1326	1.3758
120	100.4374	0.2145	0.5255
150	118.9246	0.2145	-0.5255
180	133.8811	0.1326	-1.3758
210	139.5940	0.0000	-1.7005
240	133.8811	-0.1326	-1.3758
270	118.9246	-0.2145	-0.5255
300	100.4374	-0.2145	0.5255
330	85.4809	-0.1326	1.3758
359	79.7746	-0.0047	1.7001

Figure 15. *The values of displacement, velocity and acceleration for the lowest temperature using the Cam tax software.*

Time in Degrees (Harmonic)	Displacement at +25 °C	Velocity (m/sec) at +25 °C	Acceleration (m/sec^2) at +25 °C
30	80.0000	0.0000	0.0000
60	80.0000	0.0000	1.7055
90	85.7295	0.1330	1.3798
120	100.7295	0.2151	0.5270
150	119.2705	0.2151	-0.5270
180	134.2705	0.1330	-1.3798
210	140.0000	0.0000	-1.7055
240	134.2705	-0.1330	-1.3798
270	119.2705	-0.2151	-0.5270
300	100.7295	-0.2151	0.5270
330	85.7295	-0.1330	1.3798
359	80.0066	-0.0047	1.7051

Figure 16. *The values of displacement, velocity and acceleration for the standard temperature using the Cam tax software.*

Time in Degrees (Harmonic)	Displacement (mm) at +120 °C	Velocity (m/sec) at +120 °C	Acceleration (m/sec^2) at +120 °C
30	80.1760	0.0000	0.0000
60	80.1760	0.0000	1.7092
90	85.9182	0.1332	1.3828
120	100.9514	0.2156	0.5282
150	119.5336	0.2156	-0.5282
180	134.5668	0.1332	-1.3828
210	140.3090	0.0000	-1.7092
240	134.5668	-0.1332	-1.3828
270	119.5336	-0.2156	-0.5282
300	100.9514	-0.2156	0.5282
330	85.9182	-0.1332	1.3828
359	80.1826	-0.0047	1.7089

Figure 17. *The values of displacement, velocity and acceleration for the highest temperature using the Cam tax software.*

6. Results

The importance of the investigation of the cam's volume variations is undeniable and significant since the volume variations result in the change in the values of displacement, velocity and acceleration. Obtaining these values assist the optimized and precise design of the mechanism. Thus, calculating the values of displacement, velocity and acceleration will result in a better understanding of the cam-follower performance in the space conditions. This will significantly help in the reduction of the space satellite's imprecision in different missions such as the satellite imagery of the earth's surface. Since in the latter, even a seemingly negligible imprecision such as 0.1 percent during the antenna opening can end up in a multi-kilometer inaccuracy in the satellite imagery of the desired location. Based on the Cam tax software, the values of displacement, velocity and acceleration obtained for different rotational cam angels and three different temperatures, namely lowest (T=-100 ℃) , standard (T=25℃) and highest (T=+120℃). These values are presented in figures 15 to 17. Comparing the obtained results for the lowest temperature, it is concluded that the values of displacement, velocity and acceleration of the cam are reduced by 0.29 percent with respect to the initial cam.

For the highest temperature, these values have increased by 0.22 percent. To sum up, based on the results that are obtained, an increase or decrease in the temperature ends up in an increase or decrease in the volume of the mechanism and since this variation will cause a change in the mechanism's dimensions, it will result in the changing of displacement, velocity and acceleration diagrams. In addition, it is concluded that with the temperature drop, that causes the cam-follower mechanism's volume to decrease, the values of displacement, velocity and acceleration are reduced, proportionate to the linear thermal expansion coefficient, with respect to the initial values. Similarly, for the case of temperature rise, the values increase, proportionate to the coefficient, in comparison to the initial values.

The values of displacements of three types of cams are calculated for six different temperatures and depicted in figures 18 to 20 for different cam rotation angles.

Time in Degrees (Harmonic)	Displacement (mm) at -100 °C	Displacement (mm) at -50 °C	Displacement (mm) at 0 °C	Displacement (mm) at +25 °C	Displacement (mm) at +50 °C	Displacement (mm) at +120 °C	Percentage of changes from +25 ° C to -100 ° C	Percentage of changes from +25 ° C to +120 ° C	Percentage of changes from -100 ° C to +120 ° C
30	79.7680	79.8610	79.9540	80.0000	80.0460	80.1760			
60	79.7680	79.8610	79.9540	80.0000	80.0460	80.1760			
90	85.4809	85.5805	85.6801	85.7295	85.7788	85.9182			
120	100.4374	100.5542	100.6714	100.7295	100.7876	100.9514			
150	118.9246	119.0628	119.2016	119.2705	119.3394	119.5336			
180	133.8811	134.0365	134.1929	134.2705	134.3482	134.5668	-1.00291	1.0022	1.00512
210	139.5940	139.7560	139.9190	140.0000	140.0810	140.3090			
240	133.8811	134.0365	134.1929	134.2705	134.3482	134.5668			
270	118.9246	119.0628	119.2016	119.2705	119.3394	119.5336			
300	100.4374	100.5542	100.6714	100.7295	100.7876	100.9514			
330	85.4809	85.5805	85.6801	85.7295	85.7788	85.9182			
359	79.7746	79.8676	79.9606	80.0066	80.0526	80.1826			

Figure 18. *The values of displacement for a cam with a harmonic motion for six different temperatures using the Cam tax software.*

Time in Degrees (Cycloidal)	Displacement (mm) at -100 °C	Displacement (mm) at -50 °C	Displacement (mm) at 0 °C	Displacement (mm) at +25 °C	Displacement (mm) at +50 °C	Displacement (mm) at +120 °C	Percentage of changes from +25 ° C to -100 ° C	Percentage of changes from +25 ° C to +120 ° C	Percentage of changes from -100 ° C to +120 ° C
30	79.7680	79.8610	79.9540	80.0000	80.0460	80.1760			
60	79.7680	79.8610	79.9540	80.0000	80.0460	80.1760			
90	82.6776	82.7740	82.8704	82.9181	82.9658	83.1005			
120	98.1017	98.2159	98.3303	98.3871	98.4438	98.6038			
150	121.2603	121.4011	121.5427	121.6129	121.6832	121.8812			
180	136.6844	136.8430	137.0026	137.0819	137.1612	137.3845			
210	139.5940	139.7560	139.9190	140.0000	140.0810	140.3090	-1.00291	1.0022	1.00512
240	136.6844	136.8430	137.0026	137.0819	137.1612	137.3845			
270	121.2603	121.4011	121.5427	121.6129	121.6832	121.8812			
300	98.1017	98.2159	98.3303	98.3871	98.4438	98.6038			
330	82.6776	82.7740	82.8704	82.9181	82.9658	83.1005			
359	79.7681	79.8611	79.9541	80.0001	80.0461	80.1761			

Figure 19. *The values of displacement for a cam with a cycloidal motion for six different temperatures using the Cam tax software.*

Time in Degrees (Constant_Velocity)	Displacement (mm) at -100 °C	Displacement (mm) at -50 °C	Displacement (mm) at 0 °C	Displacement (mm) at +25 °C	Displacement (mm) at +50 °C	Displacement (mm) at +120 °C	Percentage of changes from +25 ° C to -100 ° C	Percentage of changes from +25 ° C to +120 ° C	Percentage of changes from -100 ° C to +120 ° C
30	79.7680	79.8610	79.9540	80.0000	80.0460	80.1760			
60	79.7680	79.8610	79.9540	80.0000	80.0460	80.1760			
90	91.7332	91.8400	91.9470	92.0000	92.0530	92.2026			
120	103.6984	103.8190	103.9400	104.0000	104.0600	104.2292			
150	115.6636	115.7980	115.9330	116.0000	116.0670	116.2558			
180	127.6288	127.7770	127.9260	128.0000	128.0740	128.2824			
210	139.5940	139.7560	139.9190	140.0000	140.0810	140.3090	-1.00291	1.00221	1.00512
240	127.6288	127.7770	127.9260	128.0000	128.0740	128.2824			
270	115.6636	115.7980	115.9330	116.0000	116.0670	116.2558			
300	103.6984	103.8190	103.9400	104.0000	104.0600	104.2292			
330	91.7332	91.8400	91.9470	92.0000	92.0530	92.2026			
359	80.1668	80.2603	80.3538	80.4000	80.4462	80.5769			

Figure 20. *The values of displacement for a cam with a constant velocity motion for six different temperatures using the Cam tax software.*

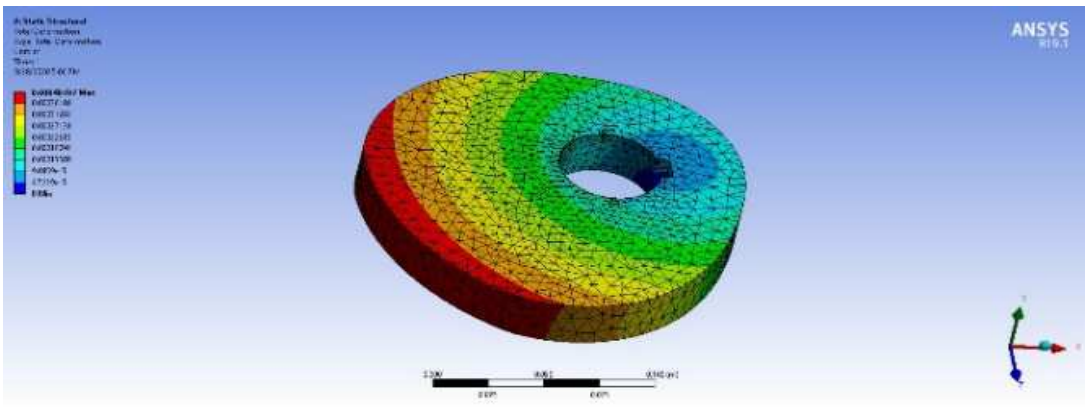

Figure 21. *The analysis of dimensional variations of a cam with harmonic motion for the lowest temperature.*

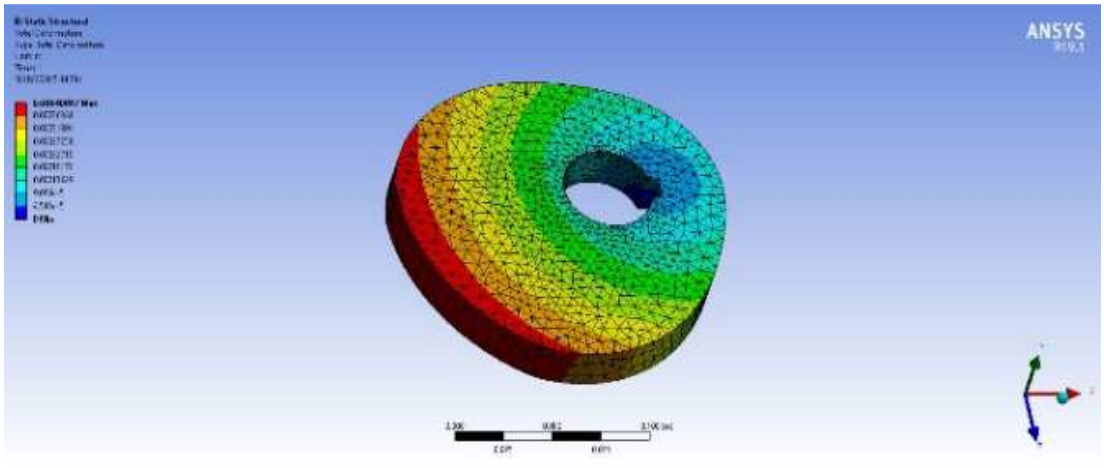

Figure 22. *The analysis of dimensional variations of a cam with cycloidal motion for the lowest temperature.*

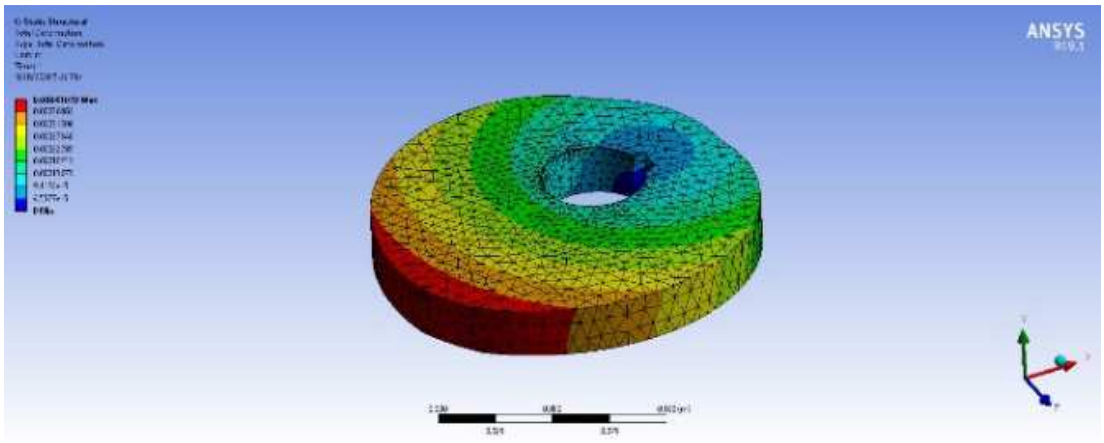

Figure 23. *The analysis of dimensional variations of a cam with constant velocity motion for the lowest temperature.*

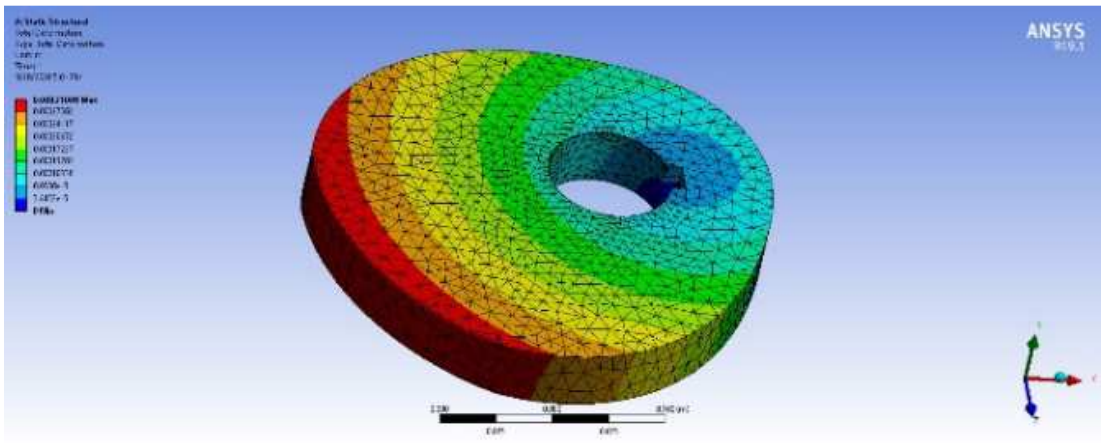

Figure 24. *The analysis of dimensional variations of a cam with constant velocity motion for the highest temperature.*

It can be concluded from the diagrams in figures 15 to 17 that although the displacement diagrams for the three types of motions are different, the increase or decrease of the displacement values with respect to the temperature variations is approximately the same between the three motion types. In other words, the motion type does not involve the intensity of displacement changes. To sum up, all three cams with different motions have an increase of dimensions by 0.22 percent when the temperature rises from +25℃ to +120℃ and have a dimension reduction by 0.29 percent when the temperature drops from +25℃ to -100℃. In other words, the cam's dimensional variation for the temperature range of -100℃ to +120℃ is 0.51 percent.

The analysis of dimensional variations caused by the temperature changes are carried out using the ANSYS software. The analysis of dimension variations caused by the temperature variations is done using the ANSYS software to compare the obtained computational results in section 2-2.

Figures 21 to 23 depict the analysis of a cam with the three types of motions for the lowest temperature. From the obtained results from ANSYS, the most dimensional change at the lowest temperature is approximately 0.407 millimeters, this number has about 0.3 percent imprecision with respect to the obtained value from the previous computations (the result obtained from ANSYS is 0.3 percent more than the computational result.). Figures 24 to 26 present the analysis of dimensional variations of a cam for the highest temperature.

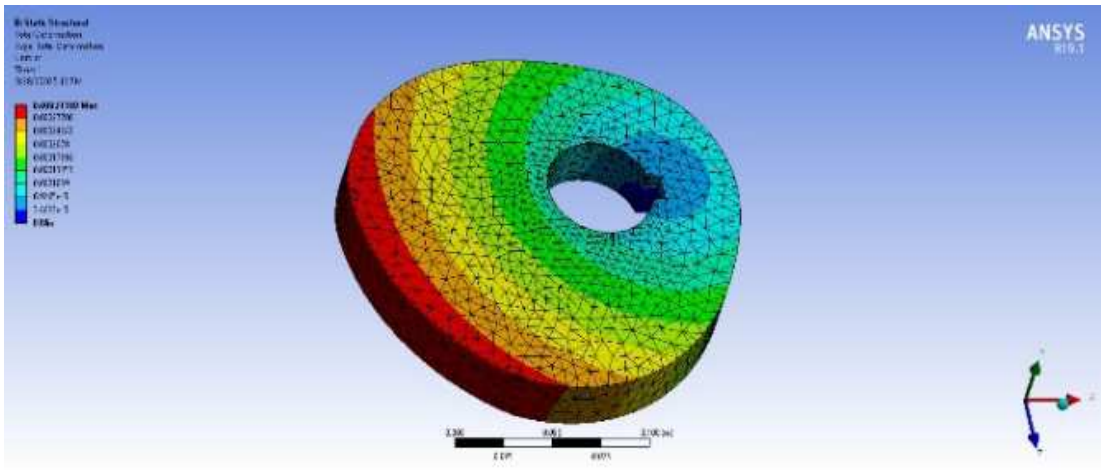

Figure 25. *The analysis of dimensional variations of a cam with cycloidal motion for the highest temperature.*

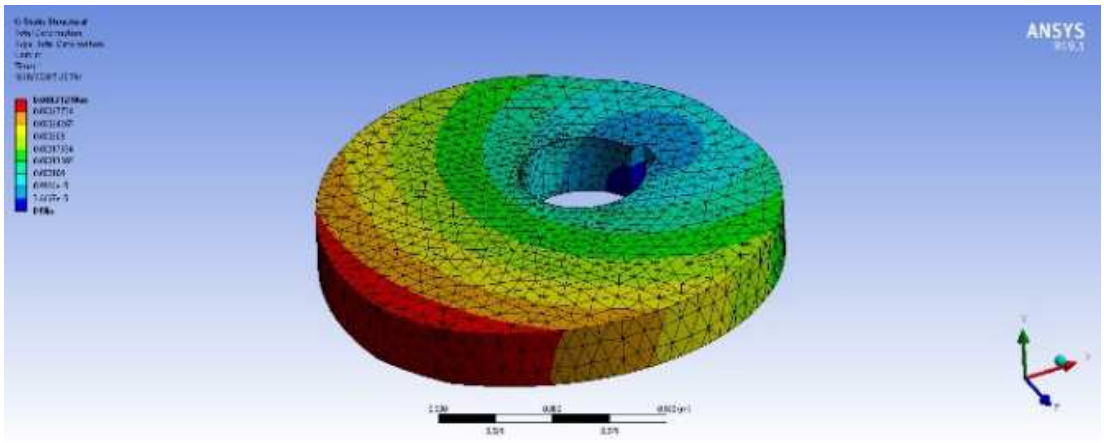

Figure 26. *The analysis of dimensional variations of a cam with constant velocity motion for the highest temperature.*

From the obtained results from ANSYS, the most dimensional change at the highest temperature is approximately 0.310 millimeters, this number has about 0.3 percent imprecision with respect to the obtained value from the previous computations (the result obtained from ANSYS is 0.3 percent more than the computational result.).

Since the imprecision has a negligible value of 0.3 percent, the calculated results are acceptable.

As stated in section 1-2-5, a solution for the temperature variation problem of the cam mechanisms is making the follower length a variable for either cases of increase and decrease in the temperature. However, it was concluded that this solution does not affect the displacement values and the displacement diagrams. There are two main reasons for this solution's impotence. Firstly, if the circumferences of the standard cam and the cams with increased and decreased volume are flattened to straight lines (as given in Figure 27), it can be seen that the three lines possess different lengths and the follower has to cover all these circumferences no matter what its length value will be. Hence, regulating the follower's length is pointless for this problem. Secondly, the cam's circumference is not a uniform shape. The cam's circumference changes all around it and when since the follower covers this distance, its length should change many times. For instance, if the follower's length changes per every ten degrees, this length change will have to occur 36 times per each complete cycle. If the cam is assumed to work for an hour, the number of times that the follower's length change must happen will be approximately 2160 times which is an almost impossible task and simply pointless. Finally, the temperature changes will not result in uniform dimensional changes in the cam. This means, the follower's length change must happen specifically for its instantaneous location on the cam's surface. Therefore, this solution is declared as incompetent for solving the temperature variation problem. Now, Investigating the design of an inclined surface for the follower is represented regarding the outcome that the proposed solution requires a servomotor mechanism.

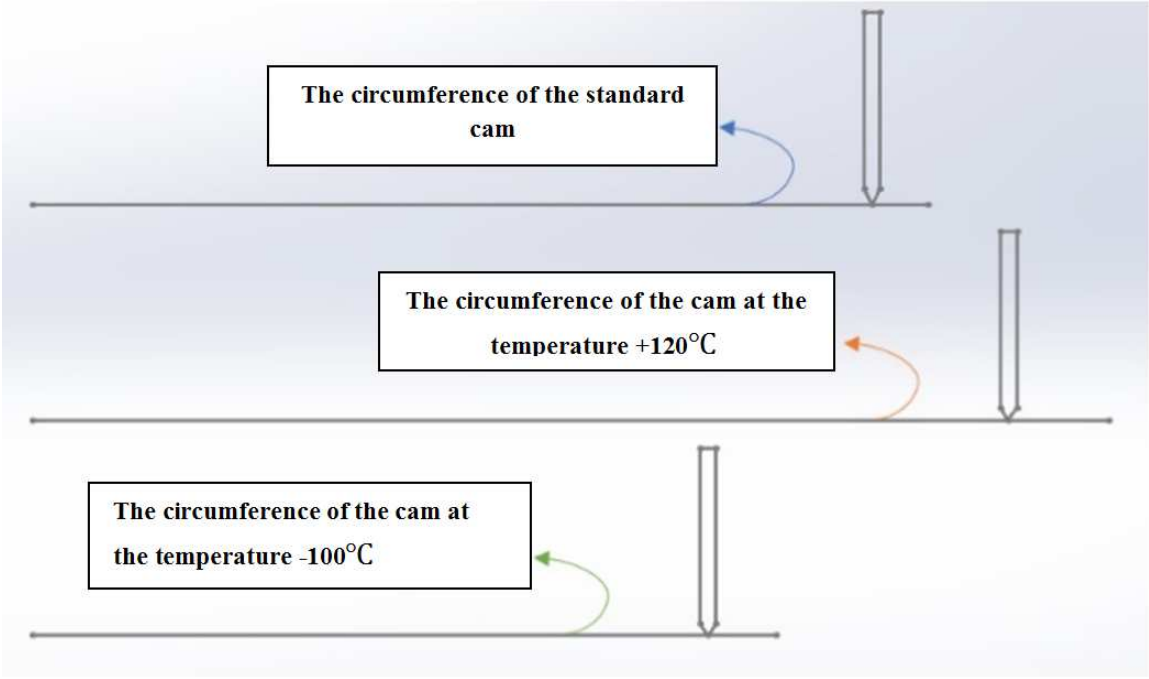

Figure 27. *The circumferences of three cams at the standard temperature, +120°C and -100°C.*

Since the problem is in space conditions, the intense temperature changes are undeniable. The minimum operating temperature of a custom-made servomotor is -50 centigrade. Thus, a servomotor won't cover the design needs as a result of the intense temperature changes. Moreover, the censors are not competent for measuring dimensional differences less than 0.01 and 0.001 millimeters. Consequently, the proposed design is economically and scientifically impossible with the present tools. Investigating the optimization of the length of a shaft connected to the cam with a ramp surface made of aluminum 7075 T6 is explained. As stated in the previous sections, the best and the most economical design for this problem is the use of expansion and contraction of metal shafts caused by temperature variations. The design is proceeded by choosing $300mm \leq L \leq 600mm$ and $3 \leq f \leq 5$. Using the optimization function *"fun"* for aluminum 7075 T6, the best optimal L is found as:

$$L = 598.699 \tag{20}$$

the optimal value for f is given as:

$$f = 3.679 \tag{21}$$

Figure 28 illustrates the variation values of the goal function when the temperature of the shaft connected to the cam with the ramp surface changes.

Using eq. (7), ΔL is obtained as:

$$\Delta L = \alpha_{Al} L \Delta T = 23.2 \times 10^{-6} \times 598.699 \times 130 = 1.806mm$$

Using equations (8), (9) and (10):

$$c^2 = (\Delta L)^2 + (\mathrm{e})^2 = (1.806mm)^2 + (0.422)^2$$

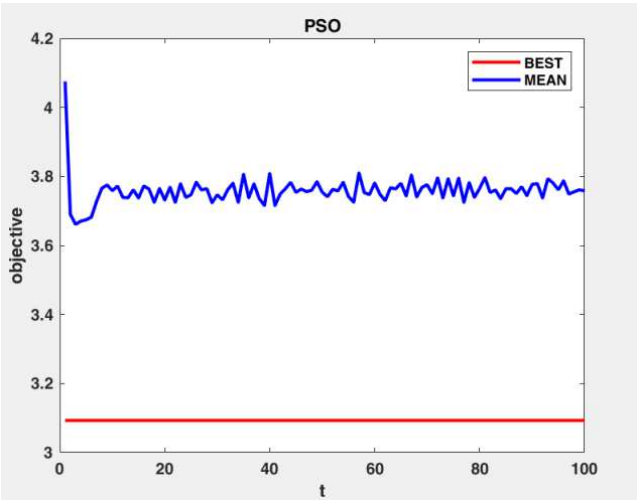

Figure 28. *Optimal values for the goal function for an aluminum cam.*

$$c = 1.855mm \tag{22}$$

For the cam's entire length:

$$\Delta L_{tot} = 2\Delta L = 2(\alpha_{Al} L \Delta T) = 2 \times 1.806 = 3.611mm \tag{23}$$

$$c_{tot} = 2c = 2 \times 1.855 = 3.71\ mm \tag{24}$$

Also:

$$e_{tot} = 2e = 2 \times 0.422 = 0.844\ mm$$

From eq. (22) it is concluded that for every 10 degrees of temperature difference, there is 0.143 millimeters displacement on the cam surface. For obtaining the cam ramp:

$$\tan\alpha = \frac{e}{\Delta L} = \frac{0.422}{1.806} = 0.234 \quad (25)$$

the angle alpha is calculated as:

$$\alpha = \tan^{-1}(0.234) = 13.17° \quad (26)$$

for the part of the cam with least dimension and most temperature difference:

$$e_a = \alpha_{Al} L_{1a} \Delta T = 23.2 \times 10^{-6} \times 80 \times 130 = 0.241mm \quad (27)$$

Similarly:

$$\tan\alpha_a = \frac{e_a}{\Delta L} = \frac{0.241}{1.806} = 0.1334 \quad (28)$$

And the angle is calculated as:

$$\alpha = \tan^{-1}(0.1334) = 7.601° \quad (29)$$

the difference between the cam's inclined surfaces is given as:

$$13.17° - 7.601° = 5.569° \quad (30)$$

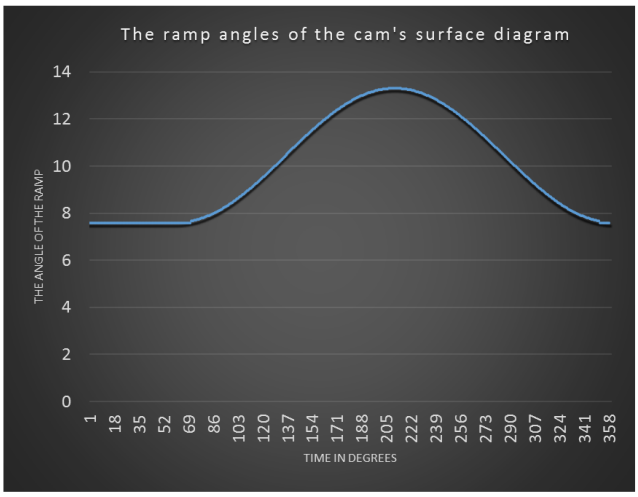

Figure 29. *The ramp angles of the cam's surface diagram of the aluminum cam.*

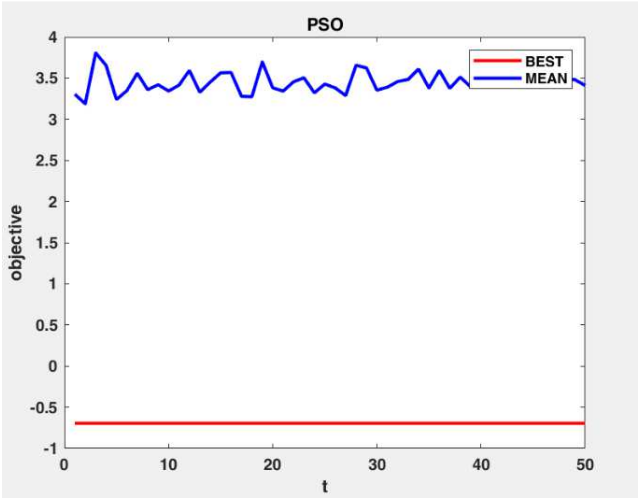

Figure 30. *The optimal values of the goal function for a titanium cam.*

By comparing the equations (26), (29) and (30) it can be concluded that the cam has a varying ramp surface that is non-linear according to the variation ratios of the cam's dimension. Specifically, this ramp angle is constant at 7.601 ° for the cam's rotation angles of 0 to 60 ° and increases non-linearly proportionate to the cam's dimensions variations to the ramp angle of the cam ratio for the cam's rotational angles 60° to 210°. The angle reaches 13.17° for the rotation angle of 210° and decreases non-linearly proportionate to the variation ratio of cam's dimensions until the rotation angle reaches zero and as a result the ramp angle reaches the angle 7.601°. Figure 29 presents the ramp angles of the cam versus the rotation angles.

It should be noted that the diagram on Figure 29 is presenting the results for the cam with a harmonic motion. And these results will certainly change for the other types of motions.

Investigation results of optimization of the length of a shaft connected to the cam with a ramp surface made of titanium is exposed here. The optimization of the titanium cam is similarly carried out which leads as follows.

Choosing $300mm \leq L_T \leq 600mm$ and $3 \leq f_T \leq 5$ and using the optimization for the defined function fun for a cam made of titanium, the most optimal length is obtained as:

$$L_T = 599.604\, mm \quad (31)$$

Also for the most optimal f_T:

$$f_T = 3.224 \quad (32)$$

Figure 30 depicts the changes of the goal function during the temperature variations of the aluminum shaft for a titanium cam with a ramp surface.

Similar to the previous part:

$$\Delta L_T = \alpha_{Al} L_T \Delta T = 23.2 \times 10^{-6} \times 599.604 \times 130 = 1.808\, mm \quad (33)$$

Also:

$$c_T{}^2 = (\Delta L_T)^2 + (e_T)^2 = (1.808mm)^2 + (0.153)^2 \quad (34)$$

And c_T is obtained:

$$c_T = 1.814\, mm \quad (35)$$

The total length of the cam is given as:

$$\Delta L_{tot} = 2\Delta L_T = 2(\alpha_{Al} L_T \Delta T) = 2 \times 1.808 = 3.616mm \quad (36)$$

Similar to the aluminum shaft:

$$(c_T)_{tot} = 2c_T = 2 \times 1.814 = 3.628\, mm \quad (37)$$

$$(e_T)_{tot} = 2e_T = 2 \times 0.153 = 0.306\, mm$$

From eq. (35) it is concluded that for every 10 degrees of temperature difference, there is 0.139 millimeters displacement on the cam surface.

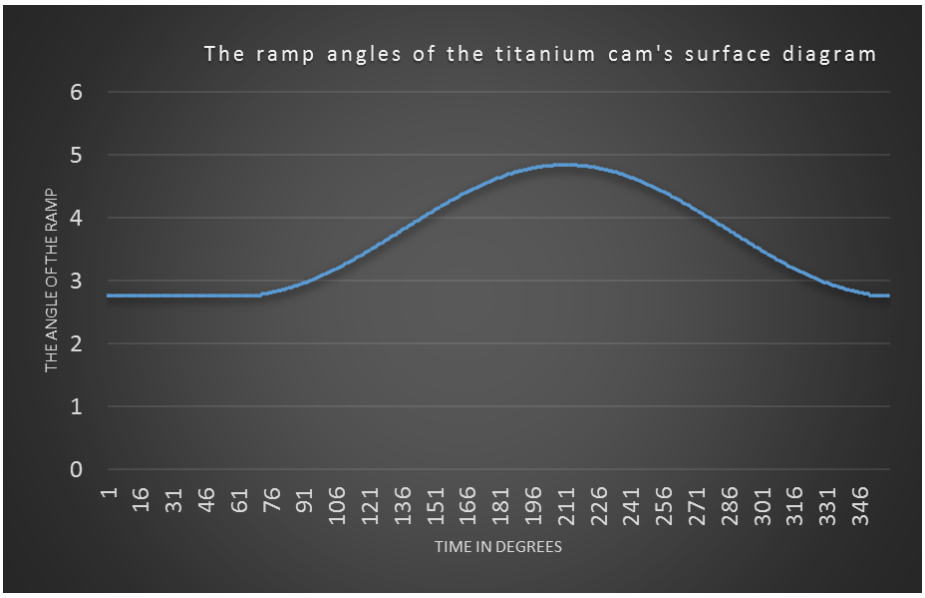

Figure 31. *The ramp angles of the cam's surface diagram of the titanium cam.*

For obtaining the cam ramp:

$$\tan \alpha_T = \frac{e_T}{\Delta L_T} = \frac{0.153}{1.808} = 0.085 \quad (38)$$

the angle alpha is calculated as:

$$\alpha_T = \tan^{-1}(0.085) = 4.86° \quad (39)$$

After comparing the results obtained by optimization of aluminum and titanium, unexpectedly for a less coefficient of linear thermal expansion the precision decreases.

In other words, the greater the coefficient of linear thermal expansion, the greater the precision.

This means that since the ramp angle of the titanium cam is 63.1 percent less than the ramp angle of the aluminum cam, the precision of the aluminum cam with respect to the titanium cam is 14.1 percent more.

For the part of the cam with least dimension and most temperature difference:

$$(e_T)_a = \alpha_T L_{1a} \Delta T = 8.41 \times 10^{-6} \times 80 \times 130 = 0.0875mm \quad (40)$$

Similarly:

$$\tan(\alpha_T)_a = \frac{(e_T)_a}{\Delta L_T} = \frac{0.0875}{1.808} = 0.0484 \quad (41)$$

And the angle is calculated as:

$$\alpha = \tan^{-1}(0.0484) = 2.771° \quad (42)$$

the difference between the cam's ramp surfaces is given as:

$$4.86° - 2.771° = 2.089° \quad (43)$$

By comparing the equations (42), (43) and (39) it can be concluded that the titanium cam has a varying ramp surface that is non-linear according to the variation ratios of the cam's dimension. Specifically, this ramp angle is constant at 2.771°for the cam's rotation angles of 0 to 60°and increases non-linearly proportionate to the cam's dimensional variations to the ramp angle of the cam ratio for the cam's rotational angles 60° to 210°. The angle reaches 4.86° for the rotation angle of 210 ° and decreases non-linearly proportionate to the variation ratio of cam's dimensions until the rotation angle reaches zero and as a result the ramp angle reaches the angle 2.771°. Figure 31 presents the ramp angles of the titanium cam versus the rotation angles.

Additionally, modification of the shaft length connected to the cam with a ramp surface is easily done on the design depicted in Figure 13 by reducing the aluminum shaft's length and using the reduced length to build the follower. With this procedure, the length of the shaft connected to the cam is reduced to half. Figure 32 presents this modified design.

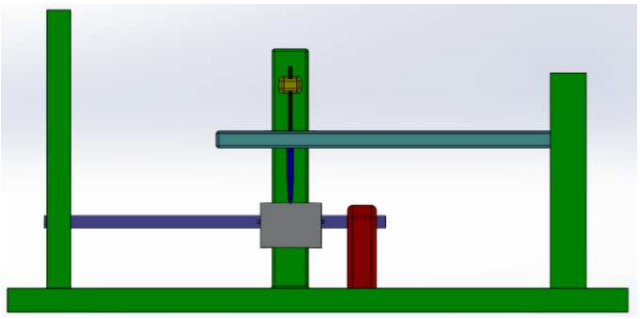

Figure 32. *The modified mechanism for the aluminum cam.*

It is vital that as depicted in Figure 33 the rod connected to the follower is not fixed at the connection point and a notch

perpendicular to the cam's shaft should be designed. Furthermore, the main follower that is connected to the rod should have the possibility to move along the shaft that is connected to the cam. In this design, there are no changes in the used parameters. The only change is the shaft's length being reduced to half. However, this reduced length is added to the length of the rod that is connected to the follower.

The function of the presented mechanism starts when the temperature rises. After the temperature rise, the shaft's length is increased and hence pushes the cam forward in its direction. Meanwhile, the length of the rod that is connected to the follower increases and pushes the follower's tip to the cam's surface and forward in the same direction with the shaft. In this design, the shaft's function is halved and the other half is handled by the length of the rod that is connected to the follower.

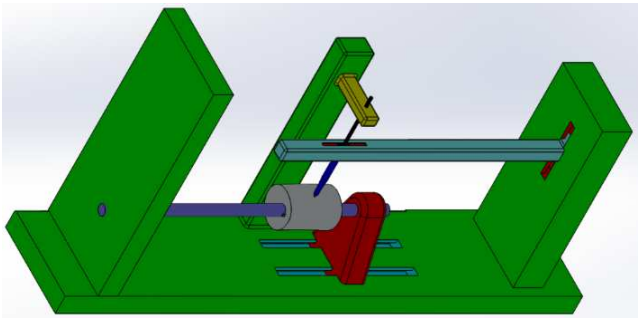

Figure 33. *Another angle of the modified mechanism.*

In order to increase the precision by double, the length of the shaft and the rod that is connected to the follower must be assumed L=598.699 millimeters. assuming the same conditions, the precision of *f*, the cam's total length ΔL_{tot} and the ramp's total length are doubled. Moreover, it can be concluded from c=3.71 millimeters that for every 10℃, there is 0.285 millimeters displacement on the cam's surface. which, half of this motion is related to the shaft's temperature variations and the other half is a result of the temperature variations of the rod that is connected to the follower.

7. Conclusion

Nowadays, the use of satellites in communication, climate, geological and military applications is significantly essential. The precision required in space imagery is highly crucial for obtaining the precise desired motions. The space's highly intense and specific condition, especially the sever temperature variation, makes space-working machines design more complicated. In this paper, difficulties caused by the intense temperature variations on space materials of satellite cam-follower mechanism are investigated and a number of impressive results were obtained. Firstly, in section 2-3 it was examined how the temperature variations affect the cams profile under different motions with the same ratios. Secondly, in section 4-3 it was concluded that changing the length of the follower cannot eliminate the temperature variation effects on the cam-follower mechanisms. In section 3-3 a comparison was made between the computational results from section 2 and the results obtained using the ANSYS software and a small imprecision of 0.3 percent between the two meths results validated the obtained results. In section 5-3 a new type of cam-follower mechanism was presented to investigate the temperature variations effects on the cam profiles that were made with a ramp surface. In sections 6-3 and 7-3, a modified design was presented to improve the previous design. In section 3-3, it was concluded that, the increase and decrease in temperature results in a change of cam's volume and as a result the cam's dimensions, displacement, velocity and acceleration values. Moreover, it was concluded that with a drop of the temperature down, the cam's volume and therein specifications are reduced proportional to the coefficient of linear thermal expansion. Similarly, the opposite result is obtained by increase of temperature. Besides, it was concluded that different motion types show different changes in displacement values due to the temperature variations. However, the ratio of these changes was the same for all the three types of motions. By comparing the results obtained in sections 6-3 and 7-3, it was concluded that the precision increases with the increase of thermal expansion coefficient. Specifically, the surface ramp angle of the titanium cam is 63.1 percent less than the surface ramp angle of the aluminum cam. However, the precision of the aluminum cam is 14.1 percent more than the precision of the titanium cam.

References

[1] Hrones J. A., An Analysis of Dynamic Forces in a Cam-Driven System. *TRANS. ASME*, Vol. 70, pp. 473-482, July 1948.

[2] Mitchell D. B., Tests on Dynamic Forces in a Cam-Driven System. *Mechanical Engineering*, Vol. 72, pp. 467-471, June 1950.

[3] Dudley W. M., New Methods in Valve Cam Design. *SAE Quarterly Transactions*, Vol. 2, No. 7, pp. 19-33, Jan. 1948.

[4] Stoddart D. A., Polydyne Cam Design. *Machine Design*, Vol. 25, No. 1, pp. 121-135, Jan. 1953; Vol. 25, No. 2, pp. 146-154, Feb. 1953; Vol. 25, No. 3, pp. 149-164, Mar. 1953.

[5] Kwakerhaak H. and Smit J., Minimum Vibration Cam Profiles. *Journal of Mechanical Engrg. Science*, Vol. 10, No. 3, pp. 219-227, 1968.

[6] Hong-Sena Y., Wen-Teng C..: Curvature analysis of spatial cam-follower mechanisms. Mechanism and Machine Theory, Vol 34, pp. 319-339, 1999.

[7] Lindholm P., Björklund S. and Cortes M. C., Characterisation of wear on a cam follower system in a diesel engine. *Wear*, Vol. 254, pp. 1199–1207, 2003.

[8] Koser K., A cam mechanism for gravity-balancing. *Mechanics Research Communications*, Vol. 36, pp. 523–530, 2009.

[9] Koser K., A cam mechanism for gravity-balancing. Mechanics Research Communications, Vol. 36, pp. 523–530, 2009.

[10] Jianpinga S., Zhaoping T.: The Parametric Design and Motion Analysis about Line Translating Tip Follower Cam Mechanism Based on Model Datum Graph. Procedia Engineering, Vol. 23, pp. 439- 444, 2011.

[11] Hsieh J. F.: Design and Analysis of Geneva Mechanism with Curved Slots. No. 13-CSME-185, E. I. C. Accession 3643, March 2014.

[12] Willemot L., Thoreson A., Breighner R., Hooke A., Verborgt O., An K. N.: Mid-range shoulder instability modeled as a cam-follower mechanism. Journal of Biomechanics, Vol. 48, pp. 2227–2231, 2015.

[13] Safaeifar H.; Design of cam and its synthesis. Applied Mathematics in Engineering, Management and Technology, pp. 145-151, Aug 2014.

[14] Hejma P., Svoboda M., Kampo J., Soukup J.: XXI International Polish Slovak Conference "Machine Modeling and Simulations 2016". Procedia Engineering, Vol. 177, pp. 3 – 10, 2017.

[15] Lin D. Y., Hou B. J., Lan C. C.: A balancing cam mechanism for minimizing the torque fluctuation of engine camshafts. Mechanism and Machine Theory, Vol. 108, pp. 160–175, 2017.

[16] Khonsari M., Torabi A., Akbarzadeh S., Salimpourb M. R.: On the running-in behavior of cam-follower mechanism. Tribology International, Vol. S0301-679X, pp. 49-80, 2017.

[17] Karamis M. B., Cerit A. A., Selcuk B., Nair F.: The effects of different ceramics size and volume fraction on wear behavior of Al matrix composites (for automobile cam material). Wear, Vol. 289, pp. 73–81, 2012.

[18] M. Hosseini-Pishrobat and J. Keighobadi, "Robust output regulation of a triaxial MEMS gyroscope via nonlinear active disturbance rejection," Int. J. Robust Nonlinear Control, vol. 28, no. 5, pp. 1830–1851, Mar. 2018, doi: 10.1002/rnc.3983.

[19] M. Hosseini-Pishrobat, J. Keighobadi, "Extended State Observer-Based Robust Nonlinear Integral Dynamic Surface Control for Triaxial MEMS Gyroscope", Robotica, November 2018, DOI: 10.1017/S0263574718001133.

[20] Keighobadi J, Hosseini-Pishrobat M, Faraji J, Langehbiz MN. Design and experimental evaluation of immersion and invariance observer for low-cost attitude-heading reference system. IEEE Trans Ind Electron. 2020; 67 (9): 7871-7878.

[21] J. Keighobadi, M. J. Yazdanpanah, and M. Kabganian, "An enhancedfuzzy H∞ estimator applied to low-cost attitude-heading referencesystem," Kybernetes, vol. 40, no. 1/2, pp. 300–326, Mar. 2011, doi: 10.1108/03684921111118068.

[22] Hosseini-Pishrobat M, Keighobadi J, Pirastehzad A, Javad Yazdanpanah M. Immersion and invariance-based extended state observer design for a class of nonlinear systems. Int J Robust Nonlinear Control. 2021; 1–22.

[23] J Keighobadi, M Hosseini-Pishrobat, J Faraji "Adaptive neural dynamic surface control of mechanical systems using integral terminal sliding mode", Neurocomputing, olume 379, Pages 141-151, 2020.

[24] J. Keighobadi, M. Hosseini-Pishrobat, J Faraji, Atta Oveisi, Tamara Nestorović "Robust nonlinear control of atomic force microscope via immersion and invariance" Int J Robust Nonlinear Control, 10 December 2018 https://doi.org/10.1002/rnc.4421

[25] M. R. Moghanni, A. Ghanbary and J. Keighobadi, "Trajectory Tracking Control of a Class of Underactuated Mechanical Systems with Nontriangular Normal Form Based on Block Backstepping Approach" J. Intell Robot Syst (2019), Accepted.

[26] S. Rafatnia, Nourmohammadi, J. Keighobadi, Badamchizadeh, "In-move aligned SINS/GNSS system using recurrent wavelet neural network (RWNN)-based integration scheme" Mechatronics, Volume 54, October 2018, Pages 155-165.

[27] M. Hosseini-Pishrobat, J. Keighobadi, Atta Oveisi, Tamara Nestorović, "Robust Linear Output Regulation Using Extended State Observer" Mathematical Problems in Engineering, Jul 2018.

[28] M. Hosseini-Pishrobat, & J. Keighobadi "Robust Vibration Control and Angular Velocity Estimation of a Single-Axis MEMS Gyroscope Using Perturbation Compensation, J. Intell Robot Syst (2018). https://doi.org/10.1007/s10846-018-0789-5

[29] H. Nourmohammadi, J. Keighobadi, GPS Solut (2018) 22: 65. https://doi.org/10.1007/s10291-018-0732-z

[30] A. Oveisi, M. Hosseini-Pishrobat, T. Nestorović, J. Keighobadi, "Observer-Based Repetitive Model Predictive Control in Active Vibration Suppression", Structuul Control and Health Monitoring, Vol. 25, May 2018.

[31] H. Nourmohammadi, J. Keighobadi, Fuzzy adaptive integration scheme for low-cost SINS/GPS navigation system, MSSP, Vol. 99, pp. 434-449, 2018.

[32] J. Keighobadi, H. Vosoughi,& J. Faraji, "Design and implementation of a model predictive observer for AHRS", GPS Solut (2018) 22: 29. https://doi.org/10.1007/s10291-017-0696-4

[33] MR Azizi, J Keighobadi. "Point stabilization of nonholonomic spherical mobile robot using nonlinear model predictive control. Robotics and Autonomous Systems" 98, 347-359, 2017. https://doi.org/10.1016/j.robot.2017.09.015

[34] H. Nourmohammadi, J. Keighobadi, Decentralized INS/GPS system with MEMS-grade inertial sensors using QR-factorized CKF, IEEE Sens. J., 17 (11) (2017), pp. 3278-3287, 10.1109/JSEN.2017.2693246.

[35] J. Keighobadi; A. H. Najafi, Full-state-feedback, fuzzy type I and fuzzy type II control of MEMS accelerometer, J Mech Sci Technol (2018) 32: 793. https://doi.org/10.1007/s12206-018-0127-z.

[36] J. Keighobadi, J. Fraji, S. Rafatnia, "Chaos Control of Atomic Force Microscope System Using Nonlinear Model Predictive Control", JOURNAL OF MECHANICS, 2016 (In Press), DOI: 10.1017/jmech.2016.89.

[37] M. Hosseini, J. Keighobadi, "Force-balancing model predictive control of MEMS vibratory gyroscope sensor" Proceedings of the Institution of Mechanical Engineers, Part C: Journal of Mechanical Engineering Science, 2015 (in press), DOI: 10.1177/0954406215607899.

[38] H. Nourmohammadi, J. Keighobadi and Mohsen Bahrami, "Design, dynamic modelling and control of a bio-inspired helical swimming microrobot with three-dimensional manoeuvring" Article in Transactions of the Institute of Measurement and Control 1 (1): 1-10 February 2016,· DOI: 10.1177/0142331215627006.

[39] J. Keighobadi and M. J. Yarmohammadi, “New chatter free sliding mode synchronization of steer by wire system under chaotic condition” Journal of Mechanical Science and Technology volume 30, pages 3829–3834 (2016).

[40] J. Keighobadi and M. R. Azizi, “Robust Sliding Mode Controller for Trajectory Tracking and Attitude Control of a Nonholonomic Spherical Mobile Robot”, AIJ-MISC, 2015.

[41] H. Millanchian, J. Keighobadi and H. Nourmohammadi, “Magnetic Calibration of Three-Axis Strapdown Magnetometers for Applications in Mems Attitude-Heading Reference Systems” AIJ-MISC, 2015.

[42] N. musavi, J. Keighobadi, “Adaptive Fuzzy Neuro-Observer Applied to Low Cost INS/GPS” Applied Soft Computing Volume 29 Issue C April 2015 pp 82–94, https://doi.org/10.1016/j.asoc.2014.12.024.

[43] T. S. Mehni, J. Keighobadi and M. B. Menhaj, "Robust predictive control of lambda in internal combustion engines using neural networks", Archives of Civil and Mechanical Engineering, Vol 13, Issue 4, December 2013, pp 432–443.